Incorporation of Oxidized Uranium into Fe (hydr)oxides during Fe(II) Catalyzed Remineralization

Peter S. Nico[1*], Brandy D. Stewart[2†], and Scott Fendorf[2]

[1]Earth Sciences Division, Lawrence Berkeley National Laboratory, Berkeley, CA 94720; 510-486-7118; 510-486-5686 (fax); psnico@lbl.gov
[2]Environmental Earth System Science, Stanford University, Stanford, CA 94305

[†]Present address: Chemical and Biological Engineering, Montana State University, Bozeman, MT 59717

Abstract

The form of solid phase U after Fe(II) induced anaerobic remineralization of ferrihydrite in the presence of aqueous and absorbed U(VI) was investigated under both abiotic batch and biotic flow conditions. Experiments were conducted with synthetic ground waters containing 0.168 mM U(VI), 3.8 mM carbonate, and 3.0 mM Ca^{2+}. In spite of the high solubility of U(VI) under these conditions, appreciable removal of U(VI) from solution was observed in both the abiotic and biotic systems. The majority of the removed U was determined to be substituted as oxidized U (U(VI) or U(V)) into the octahedral position of the goethite and magnetite formed during ferrihydrite remineralization. It is estimated that between 3% and 6% of octahedral Fe(III) centers in the new Fe minerals were occupied by U(VI). This site specific substitution is distinct from the non-specific U co-precipitation processes in which uranyl compounds, e.g. uranyl hydroxide or carbonate, are entrapped with newly formed Fe oxides. The prevalence of site specific U incorporation under both abiotic and biotic conditions and the fact that the produced solids were shown to be resistant to both extraction (30 mM $KHCO_3$) and oxidation (air

for 5 days) suggest the potential importance of sequestration in Fe oxides as a stable and immobile form of U in the environment.

Introduction

Hazardous levels of uranium in soils, sediments, and waters are present throughout the world as a result of natural deposits, mining activities, and nuclear weapons production. Uranium speciation is dominated by two oxidation states with markedly different properties. Uranium(VI), as the uranyl ion UO_2^{2+}, is the thermodynamically stable form of U in solution under oxic conditions. Uranyl adsorption onto solids such as Fe (hydr)oxides can be appreciable, but the process subject to changes in aqueous conditions and largely reversible [1-5]. In particular, CO_3^{2-}, especially in combination with Ca^{2+} or, to less extent, Mg^{2+}, suppresses adsorption (or enhances desorption) and increases mobility of U(VI) [1, 6-11].

Because reduction of U(VI) to U(IV), which forms the sparingly soluble solid UO_2 (uraninite), also decreases dissolved U concentrations, appreciable research has been devoted to understanding and exploiting this process for remediation purposes [12-15]. However, the extent of U(VI) bioreduction decreases dramatically and its tendency to reoxidize increases by coupled complexation with CO_3^{2-} and Ca^{2+} [11, 15-19]. Furthermore, common oxidants, ranging from Fe(III) to NO_3^- to O_2, can reoxidize microbially produced UO_2 [19-22]. Thus, although large quantities of soluble U(VI) can be (temporarily) bioreduced and immobilized as UO_2, maintaining a high concentration of reduced U over the long-term (decades to centuries) remains technically challenging.

Alternatively, U has been shown to coprecipitate with Fe in many environments and over a wide range of time scales including: Egyptian Fe deposits, 150-4100 ka Hawaiian soils, Fe nodules down gradient of the Australian Koongarra U deposit, and the DOE Oak Ridge site

(where uranium bearing goethite was identified) [23-26]. Investigations of U(VI) reaction with Fe(0) provide further evidence for the importance of the iron co-precipitation pathway for the uptake of U [27]. Infrared analysis indicates U associated with Fe (hydr)oxide corrosion products is probably co-precipitated as a U-Fe (hydr)oxide phase [27, 28]. Thus, both field and laboratory studies indicate that co-precipitation of U(VI) with crystalline Fe oxides formed during biotic or abiotic transformation of Fe (hydr)oxides maybe a natural attenuation pathway that can be stable on geologic time scales. However the details of this process and of the products formed are largely unknown.

In many of the studies described above, U is co-precipitated as distinct uranyl (UO_2^{2+}) phases, e.g. uranyl hydroxide or carbonate, entrapped by the host Fe oxide. However, there is also evidence of a site specific incorporation of non-uranyl oxidized U into the Fe oxides. Duff, et al. [29] reported the incorporation of U(VI) as U^{6+} during laboratory synthesis of hematite (albeit under elevated temperatures, 70^0C). Herein, we determine whether this site specific substitution of U into Fe oxides can be achieved during the abiotic and biotic Fe(II) catalyzed recrystallization of the amorphous Fe oxide ferrihydrite. The experimental conditions approximating field environments were employed to determine if site specific U substitution could be a significant natural process.

MATERIALS AND METHODS

Uranium(VI) Incorporation Experiments

Batch systems contained ferrihydrite-coated sand (1% Fe by weight; 4.8 ± 0.1 m^2g^{-1}; see Supporting Information for preparation details), PIPES (Piperazine-1,4-bis(2-ethanesulfonic acid) buffered distilled-deionized (DDI) water, uranyl acetate, $CaCl_2$, $KHCO_3$, and varying concentrations of ferrous sulfate. Solutions were made anoxic by boiling and cooling under a stream of N_2 (80%):CO_2 (20%) gas and reactions were performed under anoxic conditions in a

glovebag (Coy Laboratory Products) with a N_2 (95%):H_2 (5%) atmosphere. Each 125 mL serum vial contained 1.0 g of ferrihydrite-coated sand (10 mg Fe) and 100 mL of media buffered at pH 7 with: 3.8 mM $KHCO_3$, 0.168 mM uranyl acetate, and 3.0 mM $CaCl_2$. All systems were allowed to pre-equilibrate for 1 h prior to the addition of Fe(II) (as $FeSO_4$) at concentrations of 3 or 10 mM. Initial Fe(II) to Fe(III) molar ratios were 1.7 to 1 and 5.6 to 1 for the 3 mM Fe(II) and 10 mM Fe(II) treatments respectively. Batch systems were assembled in a glovebag and then shaken at 85 rpm at 25°C outside of the glovebag. All experiments containing Fe(II) were conducted in duplicate. Systems were maintained under anoxic conditions for 5, 15, 30, or 90 d (anoxic phase) before being aerated for 5 d (oxic phase). Solids were removed from vials, rinsed with DDI water, and dried. Solids from duplicate systems were combined to provide sufficient volume for analysis. Solids were extracted with 30 mM bicarbonate for 24 h to remove a significant fraction of the adsorbed U(VI). Initial method tests on ferrihydrite and goethite showed 64% ± 6(CL_{95}) removal of the absorbed U. A portion of each solid was digested with concentrated trace metal grade HCl to quantify total uranium, iron, and calcium (ICP-OES).

Column Design and Flow Conditions

The flow experiment was conducted using a plexiglass column packed with ferrihydrite-coated sand and inoculated with dissimilatory iron reducing bacteria (*Shewanella putrefaciens* CN32) that were supplied with anaerobic synthetic groundwater containing 0.168 mM U(VI) (as uranyl acetate), 4 mM Ca^{2+}, 3 mM lactate, and buffered at pH 7 with 3 mM bicarbonate. The column was operated for 16 d at a flow rate of approximately 3 pore volumes per day, equivalent to a pore water velocity of ca. 0.6 m d^{-1} and under conditions that allowed for significant Fe reduction and biomineralization while preventing U reduction (as verified by U XANES) through complexation with Ca^{2+} and carbonate [17]. Upon harvesting, solids were divided into four sub-samples based on distance along the flow path: 1.5 to 5.0 cm, 5.0 to 10.5 cm, and 10.5 to 14.5

cm, and 14.5 to 17 cm. Solid phase analysis was conducted as described above, except that they were not extracted with 30 mM $KHCO_3$.

Solid Phase Analysis

The solid Fe speciation was determined by linear combination fitting of Fe EXAFS data as used previously [30] and described in more detail in the Supporting Information. Uranium EXAFS scans were processed using the computer programs Athena [6, 31, 32], SixPACK [33], and Feff7 [34] (Supporting Information). The conceptual physical model of uranium in these systems consists of three components: uranium is either i) adsorbed to Fe (hydr)oxide surfaces, ii) incorporated into Fe (hyrd)oxide structure, or iii) reduced to U(IV) as $UO_{2(s)}$. From these three physical scenarios, four crystallographic models were constructed. One describes surface adsorption of U(VI), two describe a mixture of adsorption and incorporation under slightly different conditions, and the fourth describes reduced uranium as UO_2. These fitting models were compared to the data and were found to provide good fits. Details of the fitting models are presented in Supporting Information, Tables S1-3.

The *Adsorbed* model was constructed from previously published results of U adsorption onto Fe (hydr)oxides [1, 3, 5, 6, 35]. It consists of an axial O shell containing two atoms, a split equatorial shell containing four shorter and two longer U-O bonds, a carbonate shell, and an Fe shell.

The *Adsorbed and Incorporated* model *1* consists of two sub-models and includes all paths from the *Adsorbed* model other than the Fe shell which was removed, and the carbonate shell which was increased from 2 C to 3 C's per U. In addition, the model includes the paths expected from U substituted for Fe in a goethite or magnetite structure. The additional paths for the *Incorporated* portion of the model were generated by taking the crystallographic data for goethite or magnetite [36] and substituting Fe with a U atom. In magnetite, the octahedral Fe

was replaced with U. The coordination numbers (CNs) within the sub-models were constrained to ideal values based on either known crystal structures [32, 36] or previously published models [1, 3, 5, 6, 35]. The Debye Waller factors (σ^2) were grouped by distance from the central atom and identity of the scattering atom. Because of the similarity of the octahedral site in goethite and magnetite, a single first shell oxygen distance was used for both incorporated sub-models.

The *Adsorbed and Incorporated* model *2* is identical to the model *1* except that the split equatorial oxygen shell for adsorbed U was consolidated into a single shell containing six oxygens. All three of these models include the appropriate multiple scatter paths (MS) for the axial O's associated with the UO_2^{2+} ion as well as for the octahedral O site in the Fe oxides. CN's, R's, and σ^2s of the MS paths are constrained to ideal values based on the appropriate single scattering path.

The *Reduced* model consists of the O and U scattering paths expected for $UO_{2(s)}$. Unlike the previous models, the CNs and σ^2s were allowed to vary freely in this model. In all cases, the total amplitude (S_0^2) was set to 0.9, while the energy offset (E_0), the appropriate CNs, and the bond distances were allowed to vary.

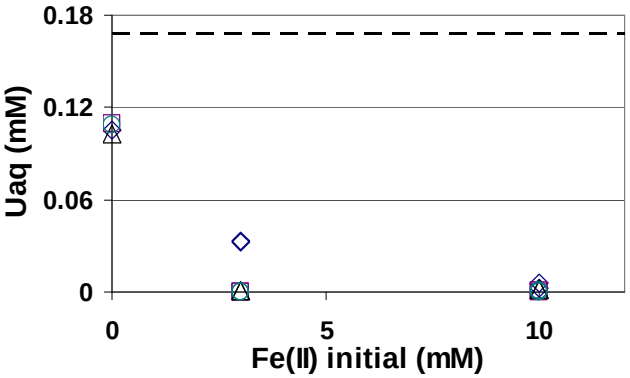

Figure 1: Aqueous phase U as a function of added Fe(II) and reaction time. Dashed line indicates initial concentration of aqueous U. Diamonds: 5 day; Triangles: 15 day; Squares: 30 day; Circles: 90 day

X-ray microprobe data were collected at the GSECARS beamline 13-ID at the Advanced Photon Source (APS) using standard data collection and processing approaches as described in the Supporting Information. Linear combination fitting of U L_{III} XANES data was performed using Sixpack [33] and spectra from: (i) the 5 d no Fe(II) reduced solid, representing U(VI) adsorbed to the surface of Fe(hydr)oxide, (ii) the 5 d 3 mM

Fe(II) oxidized solid, representing U incorporated into Fe (hydr)oxide structure, and (iii) U(IV) standard comprised of pure UO_2, representing reduced uranium.

RESULTS AND DISCUSSION

Abiotic U(VI) Incorporation

Aqueous Phase

At circumneutral pH, Fe(II) induces ferrihydrite transformation to goethite (or lepidocrocite) at low Fe(II) loadings and magnetite at high loadings [37]; for the conditions used here, reaction with 3 mM Fe(II) results in goethite formation and magnetite with 10 mM Fe(II). Upon reaction of Fe(II) (3 or 10 mM) with ferrihydrite under anoxic conditions for periods up to 90 d, $U_{(aq)}$ concentrations decrease (Figure 1); under these reaction conditions (3.0 mM Ca and 3.8 mM $KHCO_3$) the ternary Ca-UO_2-CO_3 complexes comprise >99 % of total dissolved U(VI) [11, 18]. In systems with 3 mM Fe(II), $U_{(aq)}$ decreases from 0.168 mM to below detection limit (BDL) within 15 d. At 10 mM Fe(II) $U_{(aq)}$ decreases to BDL within 5 d. In both cases, $U_{(aq)}$ concentrations remain BDL with prolonged (90 d) incubations. Without Fe(II), $U_{(aq)}$ decreases from 0.168 mM to 0.11 mM within 5 d, without further changes for periods up to 90 d. Aqueous phase Fe concentrations were similar for the 5, 15, and 30 day samples varying only between 2.3-2.4 mM for the 3 mM treatment and 6.5-6.8 mM for the 10 mM treatment. However, by 90 days aqueous Fe(II) had decreased to 1.6 mM and 2.4 mM in the 3mM and 10mM treatments, respectively see Supporting Information, Figure S1.

Solid Phase

Linear combination fitting of iron EXAFS spectra show that addition of Fe(II) induced changes in Fe mineralogy (Supporting Information: Table S5). Goethite is the only detectable transformation product after 5 d of reaction with 3 mM Fe(II) at 23% with the remainder being unreacted ferrihydrite. While not detected by Fe EXAFS, this system did show visual darkening

implying the presence of trace amounts of magnetite. When this system is aerated for 5 d, lepidocrocite becomes dominant at 31% and goethite decreases to 12%. In contrast, with 10 mM Fe(II) for 30 d, both goethite and magnetite are detected, 18% and 46%, respectively, and 5 d of aeration causes a decrease in magnetite to 15% and an increase in lepidocrocite from 0 to 21%.

Solid phase U after reaction with 3 mM Fe(II) ranges from 1.2 to 2.3 mmol kg^{-1}, decreasing to 0.84 to 1.4 mmol kg^{-1} of U in the 10 mM Fe(II) treatment (Table 1). There is a general trend toward increased solid state U concentrations with increasing anaerobic incubation time. However, this trend does not hold for the 3 mM Fe(II)-reacted, 90 d experiment—potentially an indication that the solid phase transformation has finished.

Table 1: Solid Phase U values after 5 days of aeration and extraction with 30 mM $KHCO_3$

Anaerobic Reaction Time (Days)	Solid Phase U (mmol kg^{-1})		U to Fe Mole Ratio	
	3 mM Fe(II)	10 mM Fe(II)	3 mM Fe(II)	10 mM Fe(II)
5	**1.2**	**0.84**	**0.01**	**0.006**
15	**1.7**	**0.84**	**0.01**	**0.006**
30	**2.3**	**0.91**	**0.01**	**0.005**
90	**2.2**	**1.4**	**0.02**	**0.005**

Chemical and Structural State of Solid Phase U

The U EXAFS spectra from the 5 d no Fe(II) solid sample had an E_0 value (energy at 50% normalized XANES edge height) of 17,176.0 eV and are well fit with the *Adsorbed* model (Figure 2; Table 2). In this model, U is coordinated by 2 axial O at ~1.8 Å, a split equatorial shell of approximately 4 O at 2.32 Å and 2 O at 2.46 Å, as well as a carbonate shell represented by 2 C at 2.98 Å, and finally an Fe at 3.42 Å. The fit CN and bond distances correspond well with published values [1, 3, 5, 6, 35].

In contrast, solid phase U in the 10 mM Fe(II) systems had an E_0 value 17,174.2 eV and is best represented by the *Reduced* model representing $UO_{2(s)}$ (Figure 2E); U atoms are coordinated by a nearest neighbor oxygen shell consisting of approximately 11± 2 O at 2.30 Å, consistent with an expected 8 O at 2.37 Å in $UO_{2(s)}$, and a next nearest neighbor shell of roughly 5 U at 3.82 Å. The resultant CN of 5 is less than the expected 12 U and is likely due to the small size of the newly formed $UO_{2(s)}$. The dominance of $UO_{2(s)}$ and magnetite in the 10 mM Fe(II) systems is supported by TEM images showing distinct regions with the characteristic lattice spacings of $UO_{2(s)}$ and magnetite, 3.19 and 4.85 Å, respectively, (Supporting Information: Figure S2) and confirming that in spite of the high Ca^{2+} and carbonate concentrations U(VI) is reduced to U(IV) in the presence of 10 mM Fe(II).

The U EXAFS from the 3 mM Fe(II) treatment had an E_0 value of 17,176.4 eV and is best

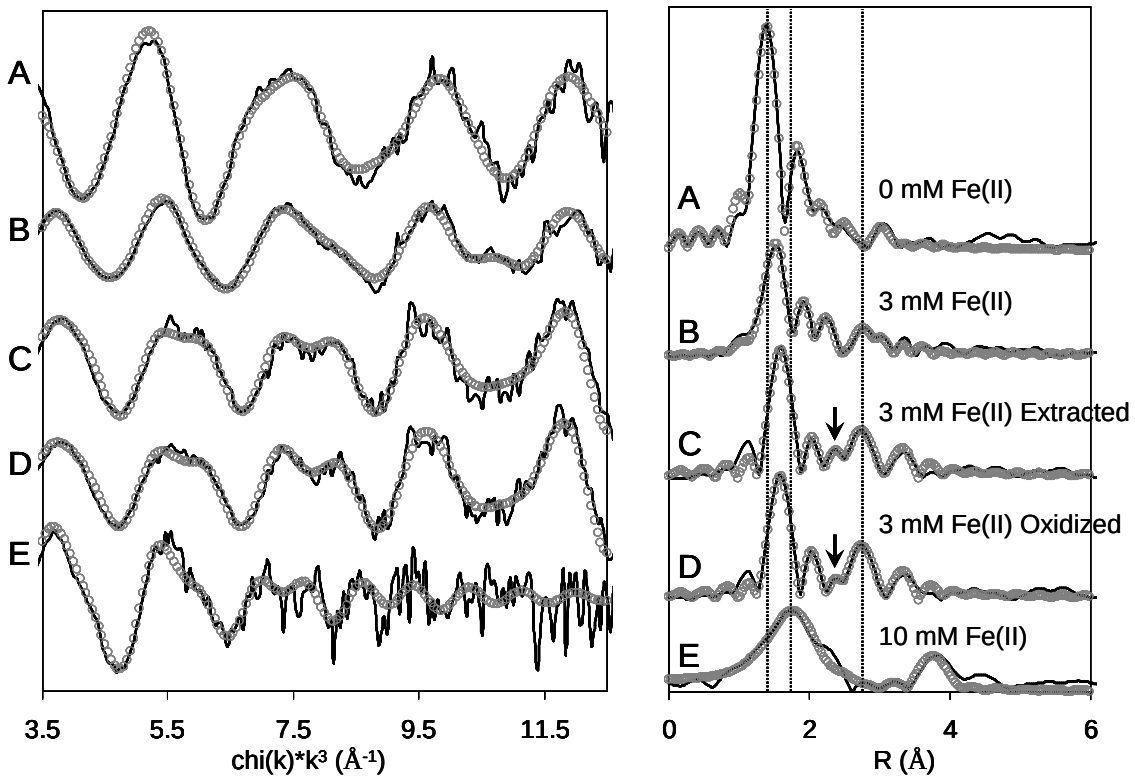

Figure 2: Uranium EXAFS data and fits for chi(k) and chi(R) functions. Solid lines represent experimental data and open circles the associated fit values.

fit by the *Adsorbed and Incorporated* model 1 (Figure 2B). This model allows for solid state U to be partitioned between two environments: U adsorbed as the uranyl ion on surfaces and U incorporated into the octahedral position of Fe oxides. The percentage of U in each phase can be estimated by comparing fit CNs to the ideal first shell coordination for the two different phases (i.e. 2 uranyl oxygens at 1.8 Å for U adsorbed and 6 O at 2.09 Å for U incorporated into goethite or magnetite). The CN of 1.6 ± 0.5 for the uranyl at 1.82 Å implies that between 55% and 100% of the U in this system is in the adsorbed phase (Table 2). Similarly, U incorporated into goethite can be distinguished from U incorporated into magnetite based on the second shell Fe; ideally there are 2 Fe at 3.02 Å for U in goethite and 6 Fe at 2.97 Å for U in magnetite. The nearest Fe distance for magnetite (0.4 ± 1 Fe at 2.8±1 Å), albeit within the range of error, implies that of the U incorporated into Fe oxides up to 23% of it could be incorporated into magnetite. Given the small percentage of U incorporated into magnetite even trace amounts of magnetite, i.e. below the Fe EXAFS diction limit, would be sufficient to accommodate this amount of U.

After extraction with 30 mM $KHCO_3$ the characteristic features of the incorporated U can more easily be distinguished (Figure 2, Table 2). These data have an E_0 value of 17,175.0 eV and are fit best with the *Adsorbed and Incorporated* model 2. The decrease in fraction of adsorbed U is noted by the decrease in the U-O CN (0.7 O at 1.83 ± 0.01 Å), indicating that only ~35% of the U in these solids is in the adsorbed phase with the remaining 65% being incorporated into Fe oxides. This 56% decrease in the amount of absorbed U is consistent with the expected ~64% efficiency of the carbonate extraction. In addition, on the basis of the 0.9 ± 0.5 Fe at 2.89 ± 0.03, between 7 and 23% of the incorporated U is bound in magnetite and the remainder incorporated into goethite. These results are also consistent with goethite being the dominant secondary mineral product in the 3 mM Fe(II) system.

Table 2: Coordination numbers (CN), bond distances (Å) for uranium EXAFS fitting. The labels in the first column identify the scattering paths associated with different solid phase forms of U. Since the first scattering shell is the same for U incorporated into goethite or magnetite, this shell is only listed once. Estimated errors are shown in parentheses. Values without error bars were derived from other variables. Full fitting parameters in Supporting Information (Tables S2 and S3).

Pathways for Different Forms of U	**Ideal Values From Literature**		**0 mM Fe E_0 = 2(1)**		**10mM Fe E_0 = 5(2)**		**3 mM Fe E_0 = 2(1)**		**3 mM Fe E_0 = 0(2) (Ext.)**		**3 mM Fe E_0 = 0(2) (Ext. and Ox.)**	
Adsorbed Uranyl	**CN**	**Distance**	**CN**	**Distance**	**CN**	**Distance**	**CN**	**Distance**	**CN**	**Distance**	**CN**	**Distance**
$U\text{-}O_{ax}$	2	1.8	1.9(1)	1.794(5)	------	------	1.6(5)	1.82(1)	0.7	1.83(1)	0.8	1.83(1)
$U\text{-}O_{eq1}$	4	2.25-2.43	3.8	2.32(2)	------	------	3.2	2.26(3)	2	2.31(3)	2.4	2.32(3)
$U\text{-}O_{eq2}$	2	2.42-2.52	1.9	2.46(2)	------	------	1.6	2.41(4)	------	------	------	------
U-C	2-3	2.86-2.91	1.9	2.98(3)	------	------	2.3	2.9(1)	1	2.8(1)	1.2	2.8(1)
U-Fe	1	3.41-3.48	0.5(7)	3.42(4)	------	------	------	------	------	------	------	------
Uraninite												
U-O	8	2.37	------	------	11(2)	2.30(2)	------	------	------	------	------	------
U-U	12	3.87	------	------	5(3)	3.82(2)	------	------	------	------	------	------
U Incorporated in Goethite or Magnetite (First Shell)												
U-O	6	2.09	------	------	------	------	2(1)	2.09(2)	3.9(4)	2.12(2)	3.6(3)	2.12(2)
U Incorporated in Goethite (Second shell)												
U-Fe	2	3.02	------	------	------	------	0.7	3.1(1)	1.0	3.08(3)	0.9	3.08(2)
U-O	1	3.23	------	------	------	------	0.3	3.23	0.5	3.23	0.5	3.23
U-Fe	2	3.28	------	------	------	------	0.7	3.2(2)	1.0	3.2(1)	0.9	3.2(1)
U-Fe	4	3.46	------	------	------	------	1.3	3.4(1)	2.0	3.58(4)	1.9	3.58(4)
Incorporated in Magnetite (Second shell)												
U-Fe	6	2.97	------	------	------	------	0.4(1.0)	2.8(1)	0.9(5)	2.89(3)	0.8(4)	2.89(3)

Lastly, 5 d of aeration prior to extraction with 30 mM $KHCO_3$ causes a small shift in the E_0 value to 17,175.4 eV but no notable alterations in the local U structure as determined by EXAFS fitting (Figure 2, Table 2) indicating that the incorporated U is unaffected by changes in redox conditions. Interestingly, there is a small decrease in the 2.42 Å peak (indicated by arrows, Figure 2C and D) and a corresponding decrease in the CN associated with the Fe shell for U incorporated into magnetite, consistent with the oxidative dissolution of magnetite. However, the change is minor and within the associated error estimates (0.9 ± 0.5 verses 0.8 ± 0.4).

Biotic Flow Experiments

Aqueous Phase

To determine if the U incorporation mechanism identified above is operable under more field relevant conditions, we conducted a biological reduction experiment under flow conditions. Iron(II) production increases steadily throughout the experiments, but always maintains a profile characterized by a peak concentration between 10 and 12.5 cm (Figure 3). Progress of the U front within the column was relatively constant at ~1 cm per day, except when the U front reaches the 10 to 12.5 cm region of the column at day 8, after which there was no detectable progression of U until day 14 (Figure 3). Uranium break-through was observed on day 16 at which point pore water concentrations throughout the first 10 cm of the column had reached values ≥0.150 mM, thus approaching the influent concentrations of 0.168 mM. Uranium concentrations beyond 10 centimeters were ≤0.100 mM.

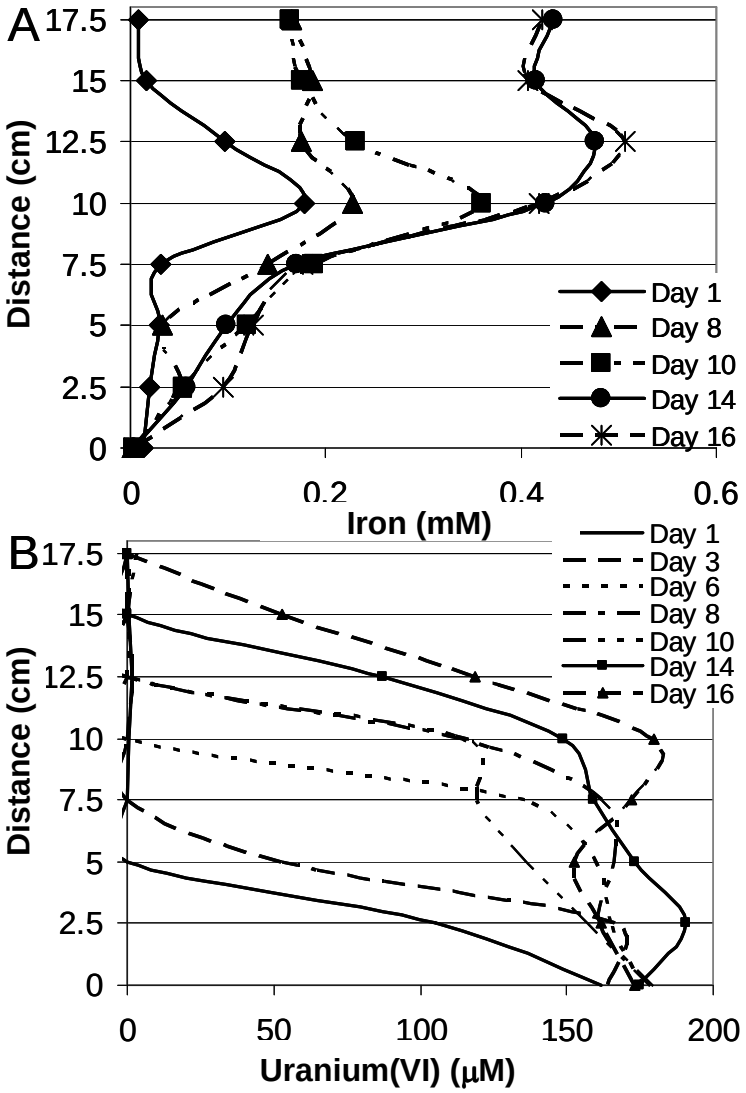

Figure 3: Pore water concentrations of A) Fe and B) U. Along the column flow path distance is relative to inlet. Port positions of 0 cm and 17.5 cm are up gradient and down gradient, respectively, of the Fe containing regions of the columns.

Solid Phase

The biogenic iron products vary along the column length, with magnetite production being maximal at 12.5 cm, driven by greater

Fe(II) concentrations in this section, Figure 3 [37]. The concentration of solid phase U shows a similar profile to biogenic magnetite, peaking at 12.5 cm, and since no reduction of U was observed by U XANES [17], suggests that U incorporation is also operable in the biotic flowing experiment. The lack of U reduction in the biotic systems as compared to the abiotic systems is likely due to the fact that the maximum Fe(II) concentration in the column is a fraction of that seen in either of the abiotic treatments. Adsorption of U onto fine grain biogenic oxides could present an alternative explanation for the correlation between magnetite formation and solid state U; however, U adsorption studies using Fe oxides containing 0 to 57% biogenic magnetite revealed no or perhaps a slightly negative correlation between U uptake and solid phase biogenic magnetite concentration (Supporting Information Table S5).

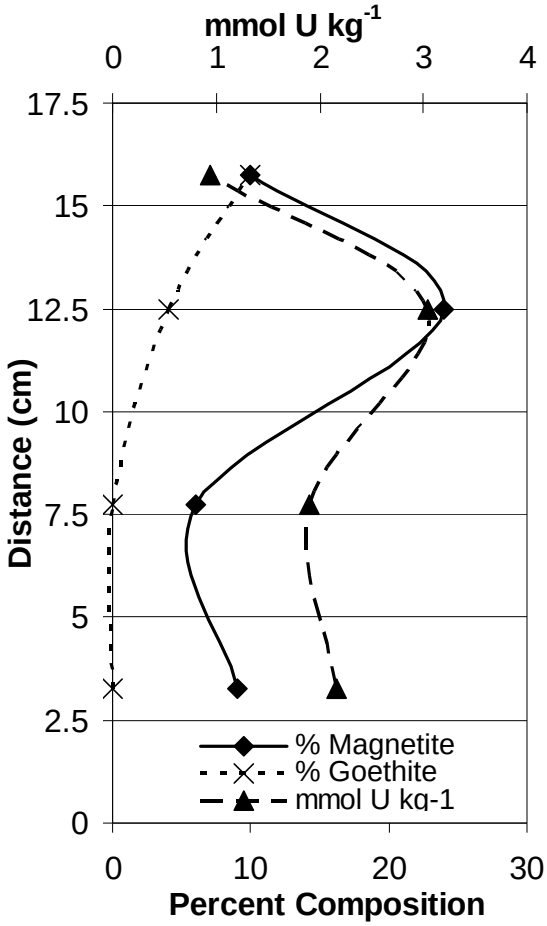

Figure 4: Solid state U (upper X axis), and percentage biogenic magnetite and goethite (lower X axis). Data points represent center of region over which column solids were homogenized: 3.25 cm (1.5 to 5.0 cm); 7.75 cm (5.0 to 10.5 cm); 12.5 cm (10.5 to 14.5 cm); 15.75 cm (14.5 to 17 cm)

Elemental maps of Fe and U distribution from the 12.5 cm section confirm the strong spatial correlation expected between U and Fe (Supporting Information). In addition, a linear combination reconstruction of a μ-XANES spectrum taken at a U hot-spot using Incorporated U, Sorbed U, and reduced U (UO_2) as standards indicates that ~32% of the U in this location is incorporated into Fe oxides with the remainder adsorbed to oxides surfaces. There was no

evidence of U(IV). TEM images, complimented with EDS analysis of these same solids, confirm the presence of magnetite with high concentrations of U, U/Fe mole ratios raging from ~2-5% (Supporting Information). Lastly, solids from the 3.25 cm and 12.5 cm sections of the column were magnetically separated and analyzed for Fe and U. In both cases, the magnetite fraction showed an increased U/Fe ratio over the bulk material from the same location, 5.6% verses 2.0%, respectively, for the 1.5 to 2.5 cm section, and 4.1% verses 2.8%, respectively, for the 8.5 to 13.5 cm section, further confirming the importance of the U substitution into magnetite.

Structural Constraints on Incorporation

The reported E_0 values for the incorporated treatments lie in the range expected of compounds containing U(V) or U(VI). Farges, et al. [38] determined that, unfortunately, there is no systematic difference in the XANES edge position between known U(V) and U(VI) containing compounds. However, using the valence bond parameters of Burns et al. [39] and the incorporated U-O octahedral bond lengths (Table 2),the calculated U valence ranges from 5.25 to 5.57, raising the possibility of a mixture of U(V) and U(VI) centers. However, when these solids underwent aeration, no changes in U-O bond length or other structural changes were detected. It would be expected that U(V) centers within the Fe matrix would have been oxidized under such conditions resulting in a change in local structure. The absence of such structural changes argues for U(VI) being the dominant form of incorporated U. However, some contribution of U(V) cannot be ruled out.

Increased structural charge resulting from substitution of U(VI) or U(V) for an Fe(III) must be accommodated either through cation vacancies, decreased protonation, or increased surface adsorbed anions. In the case of magnetite, cation site vacancies, similar to those in maghemite (γ-Fe_2O_3), could serve to maintain the charge balance. An increase in vacancies was similarly observed upon incorporation of As(V) into the magnetite structure [40]. In addition, the

deprotonation of hydroxyl groups in goethite or the reduction of near neighbor Fe(III) centers could offset the charge imbalance in goethite. However, in spite of these mechanisms, it is likely that the incorporated U center creates significant local structural distortion and that there is an upper limit to the amount of U that can be substituted into any Fe structure. However, based on the 4.1 to 5.4% U/Fe from the magnetite extractions and the 2-5% U/Fe from the TEM-EDS, this value is relatively high imply that incorporation into Fe oxides could be a significant sink for oxidized U.

The results reported here identify incorporation of U into Fe oxides as a process by which appreciable quantities of U may be sequestered under conditions where Fe (hydr)oxides are transforming to more crystalline phases. Incorporated U's resistance to both carbonate extraction and air oxidation implies that it could potentially to be stable over long time periods. If so, such a process could help to explain the strong, and long lasting, associations of U with Fe oxides in surface and subsurface environments.

Acknowledgements:

This work was supported in part by the Office of Biological and Environmental Research, Environmental Remediation Sciences Program, of the U.S. Department of Energy under Contracts No. DE-AC02-05CH11231 and ER63609-1021814, and by the Stanford NSF Environmental Molecular Science Institute (NSF-CHE-0431425), funded by the National Science Foundation Chemistry and Earth Sciences Divisions. Portions of this research were carried out at the Stanford Synchrotron Radiation Laboratory, operated by Stanford University on behalf of the U.S. Department of Energy, Office of Basic Energy Sciences and the Advanced Photon Source (U.S. Department of Energy, Office of Basic Energy Sciences under contract DE-AC02-06CH11357). GeoSoilEnviroCARS is supported by the NSF-Earth Science (EAR-0622171), Department of Energy-Geosciences (DE-FG02-94ER14466) and the State of Illinois.

Supplementary Information section includes details of EXAFS fitting, TEM images of UO_2 and U containing magnetite, X-ray microprobe elemental maps, and a micro-XANES spectrum.

References:

1. Bargar, J. R.; Reitmeyer, R.; Lenhart, J. J.; Davis, J. A. Characterization of U(VI)-carbonato ternary complexees of hematite: EXAFS and electrophoretic mobility measurements. *Geochim. Cosmochim. Acta* **2000,** *64* (16), 2737-2749.
2. Neal, A. L.; Amonette, J. E.; Peyton, B. M.; Geesey, G. G. Uranium complexes formed at hematite surfaces colonized by sulfate-reducing bacteria. *Environ. Sci. Technol.* **2004,** *38* (11), 3019-3027.
3. Reich, T.; Moll, H.; Arnold, T.; Denecke, M. A.; Henning, C.; Geipel, G.; Bernhard, G.; Nitsche, H.; Allen, P. G.; Bucher, J. J.; Edelstein, N. M.; Shuh, D. K. An EXAFS study of uranium(VI) sorption onto silica gel and ferrihydrite. *J. Electron. Spectrosc. Relat. Phenom.* **1998,** *96* (1-3), 237-243.
4. Steele, H. M.; Wright, K.; Hillier, I. H. Modelling the adsorption of uranyl on the surface of goethite. *Geochim. Cosmochim. Acta* **2002,** *66* (8), 1305-1310.
5. Moyes, L. N.; Parkman, R. H.; Charnock, J. M.; Vaughan, D. J.; Livens, F. R.; Hughes, C. R.; Braithwaite, A. Uranium uptake from aqueous solution by interaction with goethite, lepidocrocite, muscovite, and mackinawite: An X-ray absorption spectroscopy study. *Environ. Sci. Technol.* **2000,** *34* (6), 1062-1068.
6. Bargar, J. R.; Reitmeyer, R.; Davis, J. A. Spectroscopic confirmation of uranium(VI)-carbonato adsorption complexes on hematite. *Environ. Sci. Technol.* **1999,** *33* (14), 2481-2484.
7. Bernhard, G.; Geipel, G.; Reich, T.; Brendler, V.; Amayri, S.; Nitsche, H. Urany(VI) carbonate complex formation: Validation of the $Ca_2UO_2(CO_3)_{3(aq.)}$ species. *Radiochim. Acta* **2001,** *89* (8), 511-518.
8. Fox, P. M.; Davis, J. A.; Zachara, J. M. The effect of calcium on aqueous uranium(VI) speciation and absorptiong to ferrihydrite and quartz. *Geochim. Cosmochim. Acta* **2006,** *70* (6), 1379-1387.
9. Wazne, M.; Korfiatis, G. P.; Meng, X. G. Carbonate effects on hexavalent uranium adsorption by iron oxyhydroxide. *Environ. Sci. Technol.* **2003,** *37* (16), 3619-3624.
10. Zheng, Z. P.; Tokunaga, T. K.; Wan, J. M. Influence of Calcium Carbonate on U(VI) Sorption to Soils. *Environ. Sci. Technol.* **2003,** *37* (24), 5603-5608.
11. Dong, W.; Brooks, S. C. Formation of Aqueous $MgUO_2(CO_3)_3^{2-}$ Complex and Uranium Anion Exchange Mechanism onto an Exchange Resin. *Environ. Sci. Technol.* **2008,** *42* (6), 1979-1983.
12. Anderson, R. T.; Vrionis, H. A.; Ortiz-Bernad, I.; Resch, C. T.; Long, P. E.; Dayvault, R.; Karp, K.; Marutzky, S.; Metzler, D. R.; Peacock, A.; White, D. C.; Lowe, M.; Lovley, D. R. Stimulating the In Situ Activity of Geobacter Species to Remove Uranium from the Groundwater of a Uranium-Contaminated Aquifer. *Appl. Environ. Microbiol.* **2003,** *69* (10), 5884-5891.
13. Kimaro, A.; Kelly, L. A.; Murray, G. M. Synthesis and characterization of molecularly imprinted uranyl ion exchange resins. *Sep. Sci. Technol.* **2005,** *40* (10), 2035-2052.
14. Vrionis, H. A.; Anderson, R. T.; Ortiz-Bernad, I.; O'Neill, K. R.; Resch, C. T.; Peacock, A. D.; Dayvault, R.; White, D. C.; Long, P. E.; Lovley, D. R. Microbiological and geochemical heterogeneity in an in situ uranium bioremediation field site. *Appl. Environ. Microbiol.* **2005,** *71* (10), 6308-6318.
15. Gu, B. H.; Wu, W. M.; Ginder-Vogel, M. A.; Yan, H.; Fields, M. W.; Zhou, J.; Fendorf, S.; Criddle, C. S.; Jardine, P. M. Bioreduction of uranium in a contaminated soil column. *Environ. Sci. Technol.* **2005,** *39* (13), 4841-4847.

16. Barnett, M. O.; Jardine, P. M.; Brooks, S. C.; Selim, H. M. Adsorption and transport of uranium(VI) in subsurface media. *Soil Sci. Soc. Am. J.* **2000,** *64* (3), 908-917.
17. Neiss, J.; Stewart, B. D.; Nico, P. S.; Fendorf, S. Speciation-dependent microbial reduction of uranium within iron-coated sands. *Environ. Sci. Technol.* **2007,** *41* (21), 7343-7348.
18. Stewart, B. D.; Neiss, J.; Fendorf, S. Quantifying constraints imposed by calcium and iron on bacterial reduction of uranium(VI). *J. Environ. Qual.* **2007,** *36* (2), 363-372.
19. Ginder-Vogel, M.; Criddle, C. S.; Fendorf, S. Thermodynamic constraints on the oxidation of biogenic UO_2 by Fe(III) (Hydr)oxides. *Environ. Sci. Technol.* **2006,** *40* (11), 3544-3550.
20. Sani, R. K.; Peyton, B. M.; Dohnalkova, A.; Amonette, J. E. Reoxidation of reduced uranium with iron(III) (Hydr)oxides under sulfate-reducing conditions. *Environ. Sci. Technol.* **2005,** *39* (7), 2059-2066.
21. Senko, J. M.; Istok, J. D.; Suflita, J. M.; Krumholz, L. R. In-situ evidence for uranium immobilization and remobilization. *Environ. Sci. Technol.* **2002,** *36* (7), 1491-1496.
22. Wan, J. M.; Tokunaga, T. K.; Brodie, E.; Wang, Z. M.; Zheng, Z. P.; Herman, D.; Hazen, T. C.; Firestone, M. K.; Sutton, S. R. Reoxidation of bioreduced uranium under reducing conditions. *Environ. Sci. Technol.* **2005,** *39* (16), 6162-6169.
23. Dabous, A. A. Uranium isotopic evidence for the origin of the Bahariya iron deposits, Egypt. *Ore Geol. Rev.* **2002,** *19* (3-4), 165-186.
24. Pett-Ridge, J. C.; Monastra, V. M.; Derry, L. A.; Chadwick, O. A. Importance of atmospheric inputs and Fe-oxides in controlling soil uranium budgets and behavior along a Hawaiian chronosequence. *Chem. Geol.* **2007,** *244* (3-4), 691-707.
25. Sato, T.; Murakami, T.; Yanase, N.; Isobe, H.; Payne, T. E.; Airey, P. L. Iron nodules scavenging uranium from groundwater. *Environ. Sci. Technol.* **1997,** *31* (10), 2854-2858.
26. Stubbs, J. E.; Elbert, D. C.; Veblen, D. R.; Zhu, C. Electron Microbeam Investigation of Uranium-Contaminated Soils from Oak Ridge, TN, USA. *Environ. Sci. Technol.* **2006,** *40* (7), 2108-2113.
27. Eng, C. W.; Halada, G. P.; Francis, A. J.; Dodge, C. J.; Gillow, J. B. Uranium association with corroding carbon steel surfaces. *Surf. Interface Anal.* **2003,** *35* (6), 525-35.
28. Eng, C. W.; Halada, G. P.; Francis, A. J.; Dodge, C. J. Spectroscopic study of decontaminated corroded carbon steel surfaces. *Surf. Interface Anal.* **2004,** *36* (12), 1516-22.
29. Duff, M. C.; Coughlin, J. U.; Hunter, D. B. Uranium co-precipitation with iron oxide minerals. *Geochim. Cosmochim. Acta* **2002,** *66* (20), 3533-3547.
30. Hansel, C. M.; Benner, S. G.; Neiss, J.; Dohnalkova, A.; Kukkadapu, R. K.; Fendorf, S. Secondary mineralization pathways induced by dissimilatory iron reduction of ferrihydrite under advective flow. *Geochim. Cosmochim. Acta* **2003,** *67* (16), 2977-2992.
31. Newville, M. IFEFFIT: interactive EXAFS analysis and FEFF fitting. *J. Synch. Rad.* **2001,** *8* (2), 322-324.
32. Ravel, B.; Newville, M. ATHENA, ARTEMIS, HEPHAESTUS: data analysis for X-ray absorption spectroscopy using IFEFFIT. *J. Synch. Rad.* **2005,** *12* (4), 537-541.
33. Webb, S. *SixPack*, 0.52; Sam Webb: Stanford, 2002.
34. Ankudinov, A. L.; Rehr, J. J. Relativistic Calculations of Spin-dependent X-ray Absorption Spectra. *Phys. Rev. B* **1997,** *56* (4), 1712-1716.
35. Payne, T. E.; Davis, J. A.; Waite, T. D. Uranium Retention by Weathered Schists - The Role of Iron Minerals. *Radiochim. Acta* **1994,** *66/67* (1), 297-303.

36. Cornell, R. M.; Schwertmann, U., *The Iron Oxides: Structure, Properties, Reactions, Occurrences and Uses*. 2 ed.; Wiley-VCH: 2003.
37. Hansel, C. M.; Benner, S. G.; Fendorf, S. Competing Fe(II)-induced mineralization pathways of ferrihydrite. *Environ. Sci. Technol.* **2005,** *39* (18), 7147-7153.
38. Farges, F.; Ponader, C. W.; Calas, G.; Gordon E. Brown, J. Structural environments of incompatible elements in silicate glass/melt systems: II U^{IV}, U^{V}, and U^{VI}. *Geochim Cosmchim Acta* **1992,** *56* (4205).
39. Burns, P. C.; Ewing, R. C.; Hawthorne, F. C. The Crystal Chemistry of Hexavalent Uranium: Polyhedron Geometries, Bond-Valence Parameters, and Polymerization of Polyhedra. *Can Mineral* **1997,** *35*, 1551-1570.
40. Coker, V. S.; Gault, A. G.; Pierce, C. I.; Laan, C. V. D.; Telling, N. D.; Charnock, J. M.; Polya, D. A.; Lloyd, J. R. XAS and XMCD evidence for species-dependent partitioning of arsenic during microbial reduction of ferrihydrite to magnetite. *Environ. Sci. Technol.* **2006,** *40* (24), 7745-7750.